High Performance Electrochemical Saline Water Desalination using Silver and Silver-chloride Electrodes

Published as: *Desalination*, 476, 114216 (2020)
https://doi.org/10.1016/j.desal.2019.114216

Jaewuk Ahn[1], Jiho Lee[1], Seoni Kim[1], Choonsoo Kim[2], Jaehan Lee[3], P.M. Biesheuvel[4], Jeyong Yoon[*, 1]

[1]*School of Chemical and Biological Engineering, College of Engineering, Institute of Chemical Process, Seoul National University (SNU), 1 Gwanak-ro, Gwanak-gu, Seoul 08826, Republic of Korea*

[2]*Department of Environmental Engineering and Institute of Energy/Environment Convergence Technologies, Kongju National University, 1223-23, Cheonan-daero, Cheonan-si 31080, Republic of Korea.*

[3]*Department of Biological and Chemical Engineering, College of Science and Technology, Hongik University, Sejong-si 30016, Republic of Korea*

[4]*Wetsus, European Centre of Excellence for Sustainable Water Technology Oostergoweg 9, 8911 MA Leeuwarden, The Netherlands*

Jeyong Yoon (corresponding author)

E-mail: jeyong@snu.ac.kr, Phone: +82-2-880-8927, Fax: +82-2-876-8911

Keywords: seawater desalination; Faradaic electrodes; ion-exchange membrane; capacitive deionization

Abstract

Electrochemical desalination technologies such as capacitive deionization (CDI) and battery desalination (BD) are considered as promising brackish water desalination technologies because of their low energy consumption and environmental friendliness. However, it is a still challenge to develop an efficient way to deionize highly concentrated salt water using these technologies due to the limited desalination capacity. Here, we demonstrate how a system consisting of anion selective two-phase reaction battery electrodes combined with a cation exchange membrane shows a much higher capacity (approx. 85 mg g^{-1}) along with remarkable salt removal efficiency (80%) while the cell voltage is still low (0.2 V). Moreover, with this system, it is possible to operate with high currents (100 A m^{-2}) that are an order of magnitude higher than previous battery desalination systems.

Introduction

Capacitive Deionization (CDI) has emerged as a next generation of desalination technology due to its mild operation conditions, portable capability, and potential for low energy use [1–14]. The desalination performance of CDI with brackish water is competitive with conventional desalination technologies, but it is difficult for CDI to treat a high salt concentration solution because the electrodes have limited adsorption capacity [7]. The principle of CDI to remove salt ions is by ion adsorption in an electrical double layer (EDL) on the electrode surface. The adsorption capacity of EDL can be enhanced by increasing the cell voltage, but the typical CDI operating voltage is limited to around 1.2 V since at higher voltages the energy efficiency is significantly reduced by side reactions such as water decomposition [15–19].

Recently, battery electrodes using Faradaic reactions have been applied to electrochemical desalination technology [20]. By applying battery electrodes, it is possible to increase the salt removal capacity significantly because the ions are captured by chemical bonds inside the electrodes while self-discharge, the escape of ions held by the electrode without any applied electrical energy, is reduced [21]. For those reasons, many electrochemical desalination system using battery electrodes have been proposed such as hybrid capacitive deionization (HCDI) [22–24] and the desalination battery (DB) [20]. HCDI and DB, however, after a first step in which ions are adsorbed, require a regeneration step to release the ions adsorbed on electrodes. Thus, for half of the time, the device is not used to desalinate water.

To overcome this disadvantage of more conventional systems, cation intercalation desalination (CID) was proposed and experimentally verified [25–28]. In this system, a cation selective battery material is used in both electrodes, and an anion exchange membrane is placed between the two electrodes, separating the two chambers. Cations react with the negative electrode and are removed, while at the same time the positive electrode releases cations. During operation, only anions pass through the membrane to neutralize the charge imbalance in the solution in the both chambers. As a result, a characteristic of the CID mechanism is that ion capture and release occur simultaneously in each chamber, thereby giving the system continuity to the production of desalinated water. Various cation intercalation electrodes such as sodium manganese oxide (NMO) [25] and Prussian blue analogues (PBAs) [26–28] have been applied to the CID system. Nevertheless, the rate performance and desalination capacity of CID still need to be further improved to achieve higher efficiency to deionize highly concentrated salt water.

In the present work, we report how to improve the rate performance and desalination capacity from extending the concept of CID, by using electrodes made of a silver/silver chloride

composite, which are able to serve as an anion selective battery material, as also reported in ref [29–31]. Previously, our approach was presented in ref [29] and [30] while a related work with using the carbon nanotube and silver composite electrodes was recently reported by Srimuk *et al.* [31]. The salt removal efficiency, however, was less than 1% for synthesized seawater desalination in [31]. Also, Grygologwicz *et al.* [32] and Fighera *et al.* [33] used two silver/silver chloride electrodes and a cation-exchange membrane to study salt concentration changes, but this approach desalting is presumed to be difficult when applying reverse current because the channel volumes of the two system is different. **Figure 1** gives a schematic diagram of our system, which shows that silver and silver-chloride electrodes are used instead of cation intercalation electrodes (which are used in CID) to capture anions, and a cation exchange membrane is placed in the middle of the cell for the selective transport of cations. The silver and silver-chloride electrodes have been used for battery desalination and hybrid CDI because they have a high specific capacity (theoretical specific capacity of 250 mAh g^{-1}), fast kinetics, and low solubility in salt water [20,22,29–34]. With much interest in silver and silver-chloride electrodes for electrochemical desalination, reportedly silver-additions in graphene electrodes was used for enhance desalination performance of the electrode [35].

In our study, we show that desalination with Cl^- selective Ag/AgCl electrodes is possible in combination with a cation exchange membrane in a system where desalinated water is continuously produced. The performance of the system was evaluated by analyzing the salt adsorption capacity (SAC), the average salt adsorption capacity (ASAR), and the specific energy consumption (SEC) in 500 and 1000 mM NaCl solutions.

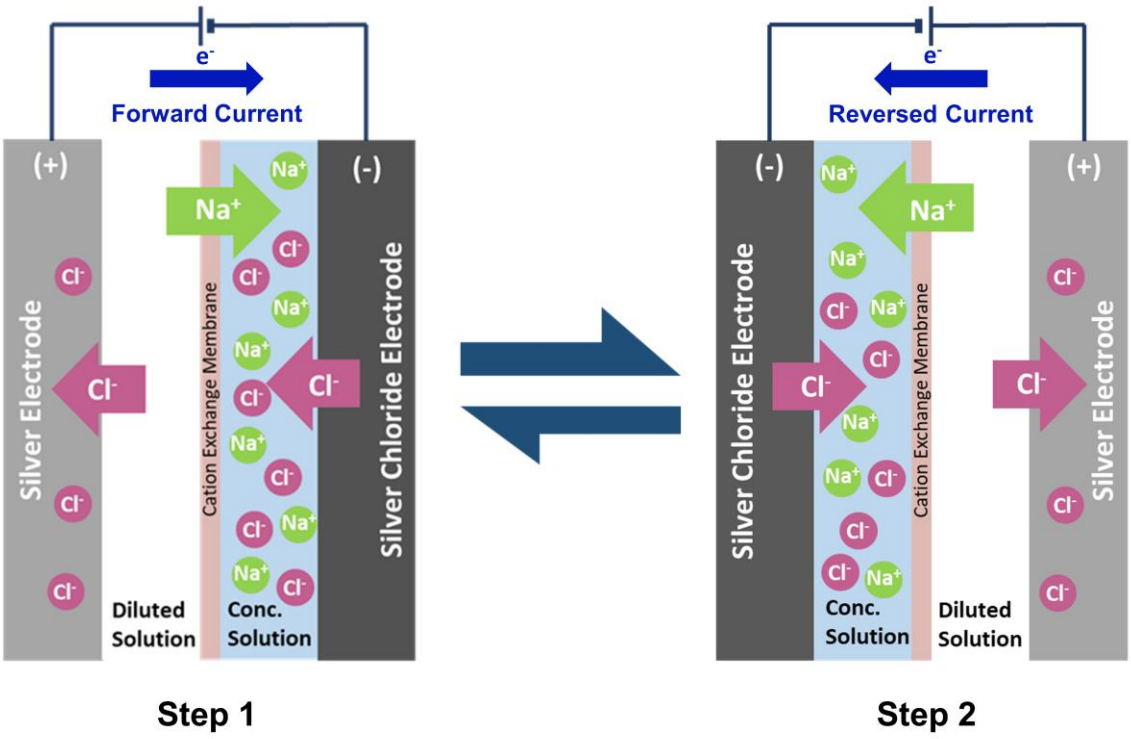

Figure 1. Schematic diagram of the electrochemical desalination cell with silver and silver-chloride electrodes.

Materials and Methods

1. Electrode Preparation

To prepare a silver electrode, 80 wt % Ag particles of an average size of 300 nm (Sigma Aldrich), 10 wt % carbon black (Super P, Timcal, Switzerland), and poly-tetrafluoroethylene (PTFE, Sigma Aldrich) were mixed gently with ethanol as solvent for 20 min. The mixture was placed on a roll presser to make an approx. 0.2 mm thickness sheet-type electrode. The fabricated silver electrode was dried in a 120 °C vacuum oven overnight to remove the residual solvent.

A three-electrodes system was employed to convert one of silver electrodes to a silver-chloride electrode. To do this, a current of 2 mA cm^{-2} was applied to the silver electrode, a working electrode, in a 1.0 M NaCl solution until the cell voltage reached 0.2 V vs. Ag/AgCl (KCl saturated) as reference electrode with a Pt mesh as counter electrode.

In order to bring the as-prepared electrodes into a dynamic equilibrium state, the electrodes were subjected to 20 cycles of cyclic voltammetry (CV) with a scan rate of 20 mv s-1 in the range of -0.6 to 0.6 V.

2. Characterization of the Electrodes

The surface morphology of the electrodes was characterized by field emission scanning electron microscopy (FESEM, JEOL JSM-6799F, Japan). The crystalline structure was analyzed by X-ray diffraction (XRD, Rigaku, Japan) in a 2θ range of 10°-80° with a ramping step of 2° min^{-1}.

CV and galvanostatic charge/discharge experiments were carried out to determine the electrochemical properties of the electrodes in 1.0 M NaCl solution in a three-electrode cell.

For both experiments, our prepared silver electrode was the working electrode and a commercial Ag/AgCl (Sat. KCl) the reference electrode, while 1.0 M NaCl solution was used as the electrolyte. The CV scan was obtained by a potentiostat (PARSTAT 2273, Princeton Applied Research, USA) with scan rates of 2, 5, 10, 20, and 30 mV s^{-1}. For the galvanostatic charge/discharge test, 1 mA cm^{-2} of constant current was applied to the cell in a range of -0.2 V to 0.2 V using a battery cycler (WBCS3000; WonA Tech, Korea).

3. Cell Construction

A schematic diagram assembled desalination cell is shown in **Figure 2**. The 2.0 cm x 2.0 cm area of the silver electrode and the silver chloride electrode were attached onto titanium plates (thickness: 0.2 mm, Sigma Aldrich) with carbon paint (DAG-T 502, Ted Pella). The cell is divided into two regions, which are named chambers A and B, by placing a cation exchange membrane (CMV, Selemion, Japan) in between two polyamide woven spacers (thickness: 0.6 mm). At the start, the silver electrode was placed in chamber A, and the silver-chloride electrode was placed in chamber B. The cell was covered with PTFE plates and 1.5 mm silicon gaskets to prevent leaking of solution. Afterwards, the cell was firmly clamped together under a uniform pressure.

4. Desalination Performance

A volume of 0.6 mL of 0.5 and 1.0 M NaCl solution was placed in each chamber (total amount of solution in the cell: 1.2 mL). The system was operated in constant current mode (±1, 3, 5, 10 mA cm^{-2}) over a voltage range of -0.2 V to 0.2 V, where the positive current was applied first to the silver electrode (step 1). When the cell voltage reached the limit that was set, the

solution in each chamber was changed to a new solution, and then a reverse current was applied to the system (step 2). The concentration of cations after each step was measured by ion chromatography (ICS-1100, Thermo Fisher Scientific Inc.). Note that ion concentration is only measured after each step, but not during the cell operation.

The desalination parameters were calculated for a full cycle consisting of a current and a reversed current step. The ion removal efficiency was calculated by

$$\text{ion removal}\ (\%) = \frac{C_i - C_t}{C_i} \cdot 100 \qquad (1)$$

where C_i is the initial ion concentration, and C_t is the desalted ion concentration

The salt adsorption capacity (SAC) was calculated by

$$\text{SAC}\ (\text{mg g}^{-1}) = \sum_i \left(\frac{MW_{NaCl}}{m_e} \cdot \Delta C_i \cdot V_c\right) \qquad (2)$$

where MW_{NaCl} is the molecular weight of NaCl (58.4 g mole^{-1}), m_e is the total weight of both electrodes (g), ΔC_i is the concentration change of i step (mM), and V_c is the volume of a chamber (mL). The summation of i is over the two steps that together form one cycle.

The average salt adsorption rate (ASAR) was calculated by

$$\text{ASAR}\ (\text{mg g}^{-1}\text{s}^{-1}) = \frac{\text{SAC}}{\Delta t} \qquad (3)$$

where Δt is the cycle time.

The specific energy consumption (SEC) can be calculated from [36]

$$\text{SEC}\ (\text{kJ mole}^{-1}) = \frac{\int_0^{t_{cycle}} I \cdot V_{cell}\, dt}{\text{moles salt removed}} \qquad (4)$$

where V_{cell} is the time dependent cell voltage, and I is the applied current (A). We integrate

over a full cycle (from time zero to the end of a cycle, t_{cycle}).

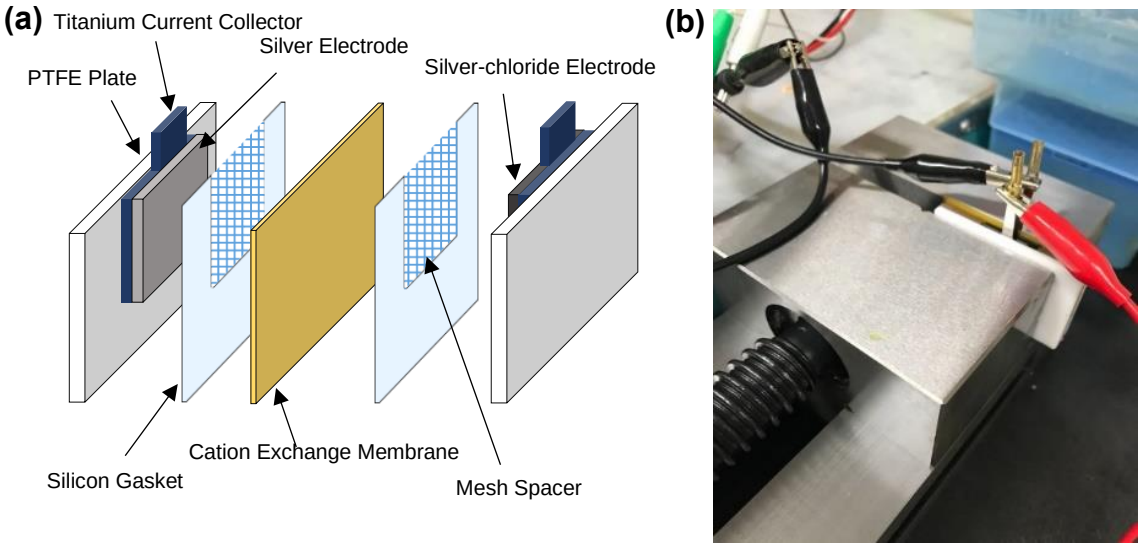

Figure 2. Laboratory-scale system for continuous water desalination with Ag/AgCl electrodes. (a) Illustration of the layout of the system, (b) Photograph of the cell construction.

Results and Discussion

Figure 3 shows that the desalination performance of the system during constant current operation with synthetic salt water (500 mM NaCl). As can be seen in **Figure 3a**, the concentration of Na^+ ions is reduced to approx. 100-110 mM in the forward current step as well as in the reversed current step. Thus, the average ion removal, ΔC, is approx. 80%. This salt removal is much higher than in ref [31] where the ion removal was always less than ΔC=1 mM. As constant current is applied to the system (**Figure 1**), the silver electrode reacts with chloride ions in one chamber, while at the same time the silver-chloride electrode releases the chloride ions in the other chamber.

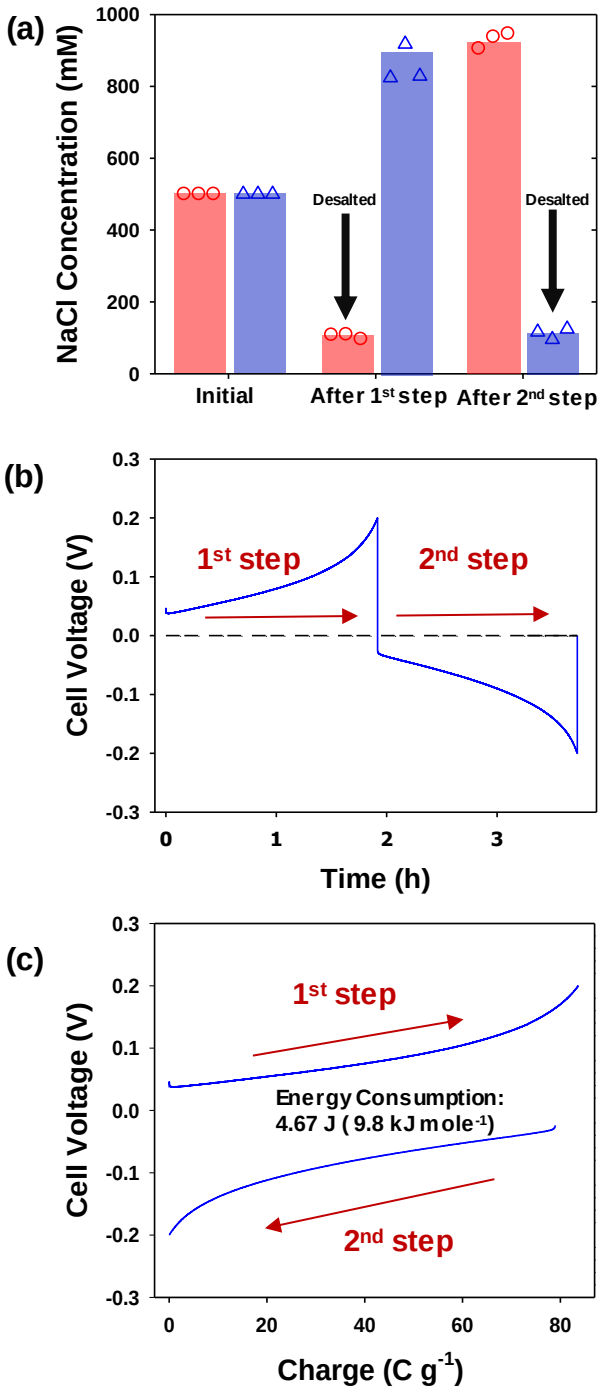

Figure 3. (a) The Na^+ concentration in the two chambers, at three moments: before the experiment, at three moments: before the experiment, after forward current, and after reverse current. (b) The cell voltage profile during the forward current (step 1) and the reversed current (step 2) step. (C) The cell voltage vs. charge plot during step desalination in 500 mM NaCl

(current density: 1.0 mA cm^{-2}).

As a consequence, the cations move through the cation exchange membrane to the chamber where chloride ions are released, to neutralize charge imbalance of the solutions. Thus, the chambers are alternatingly desalted and concentrated during the forward and reverse step. Interestingly, the system works successfully even under the low final cell voltage of 0.2 V (**Figure 3b**). That a small voltage window is sufficient, can be attributed to the reversible two-phase conversion reaction of silver and silver chloride ($Ag + Cl^- \rightarrow AgCl$, $E^0 = 0.22$ V *vs*. SHE). Consequently, because of this low cell voltage, the specific energy consumption of the system, SEC, is very low, and we calculate a value of approx. 10 kJ per of salt removed (**Figure 3c**).

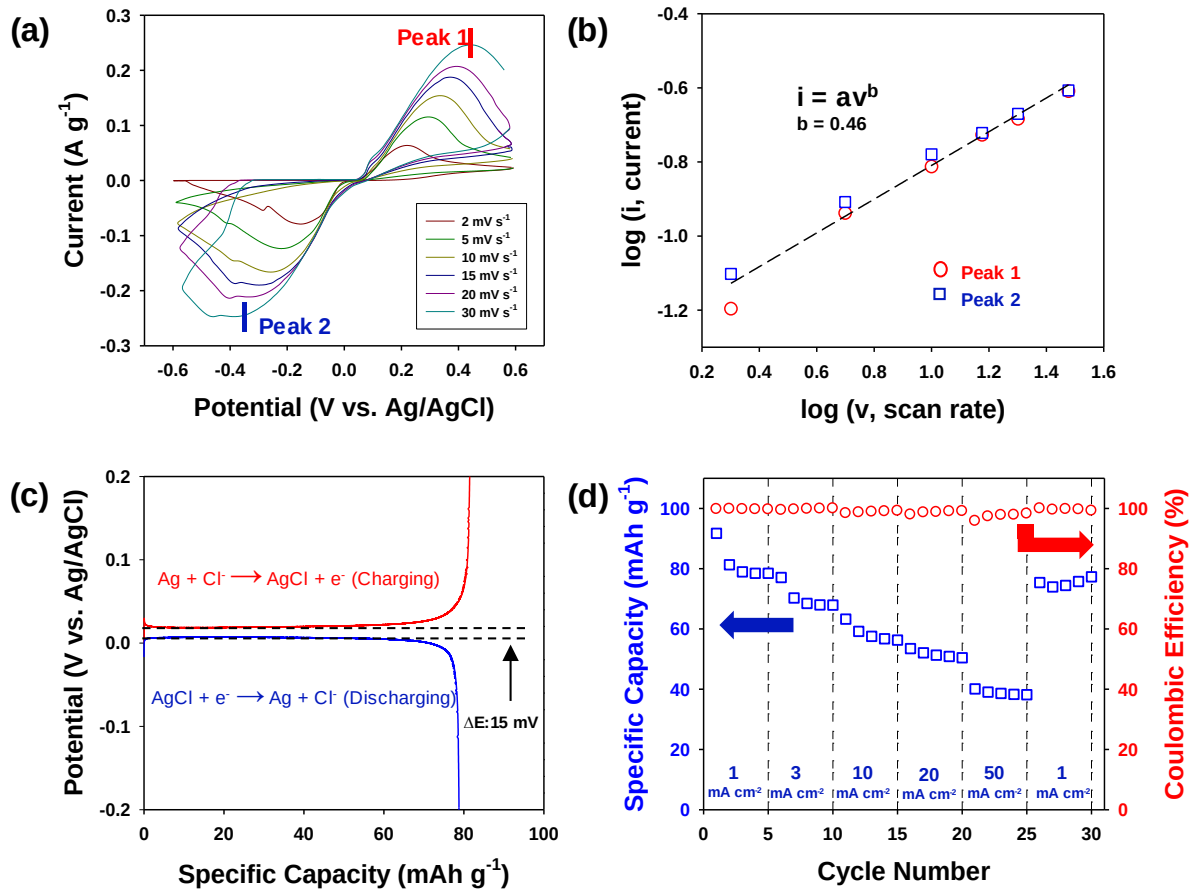

Figure 4. Electrochemical characterization of the silver/silver-chloride electrode: (a) cyclic voltammetry curves in 1000 mM NaCl solution (scan rates: 2.0 - 30 mV s^{-1}); (b) power-law relation between the peak current and the scan rate from the result of CV curves (panel (a)); (c) galvanostatic charge/discharge of the silver/silver-chloride electrode at 1000 mM NaCl solution in the three-electrode configuration (current density: 1.0 mA cm^{-2}). (d) The rate capabilities of the silver electrode in the three-electrode configuration at 1000 mM NaCl solution (current densities: 1.0, 3.0, 10, 20, and 50 mA cm^{-2}).

The electrochemical characteristics of the silver electrode were examined with cyclic voltammetry (CV) and galvanostatic charge/discharge (**Figure 4**). **Figure 4a** shows a CV curve of a silver electrode in 1000 mM NaCl solution with different scan rates. The oxidation and

reduction current of the electrode is associated with the conversion reaction of the silver electrode with Cl^- ions. As the scan rate is increased, the peak potentials of oxidation and reduction are extended while maintaining the overall shape, which is an indication of the Faradaic reaction. In order to further investigate the electrode process, we tested the power law relation, $i=a.v^b$, where i is current and v the scan rate, results of which are presented in **Figure 4b**. The calculated b value of oxidation and reduction peaks was 0.46, close to 0.5, implying that the conversion reaction of silver and silver-chloride is a diffusion-controlled reaction (the Faradaic reaction is not rate-limiting) [37].

Figure 4c shows the result of the galvanostatic charge/discharge experiment at 1 mA cm^{-2} current density. From the result in **Figure 4c**, the specific capacity of the silver/silver-chloride electrode can be derived as approx. 80 mAh g^{-1} (approx. 100 mAh g^{-1} based on active material), which is higher than for intercalation materials such as NMO (35 mAh g^{-1}) and Prussian Blue Analogues (60 mAh g^{-1}) [27]. In intercalation materials, often with each ion adsorption site a large number of atoms is associated from the lattice structure. Instead, the silver electrode, which is a conversion electrode, can react with the chloride at a ratio of 1:1, thus exhibiting a larger specific capacity than intercalation electrodes. Nevertheless, in our study, the silver electrode did not achieve the theoretical maximum capacity of 250 mAh g^{-1}. This may be owing to diffusion limitation of Cl^- ions originating from particle agglomeration during the conversion reaction from silver to silver-chloride (**Figure S1 (a) and (b)**).

In addition, the voltage profile shows a constant voltage even though the reaction proceeds, see **Figure 4c**, which is a characteristic of a two-phase reaction electrode, as explained by the Gibbs phase rule [38–40]. Two-phase reaction of the silver and silver-chloride electrode was confirmed by X-ray diffraction (XRD) as shown in **Figure S2**. Furthermore, the gap between the oxidation and reduction potential is approx. 15 mV (**Figure 4c**), which shows that the

overpotential of the silver electrode reacting with Cl^- is small. These characteristics of the silver electrode allows this system to operate at a low cell voltage (0.2 V).

Figure 4d shows the specific capacity and Coulombic efficiency of silver electrode with different current densities (1.0 to 50 mA cm^{-2}). From the capacity retention ratio (50% at a current density of 50 mA cm^{-2} compared with 1.0 mA cm^{-2}), we can conclude that the silver electrode has a good rate capability due to its rapid silver/silver chloride conversion reaction based on the small size of the Ag-particles in the electrode. In fact, the retained capacity is approx. 100% after 100 cycles tests with 3.0 mA cm^{-2} in the two-electrode configuration system at 500 mM NaCl solution (**Figure S4**), suggesting that both of electrodes, the silver and the silver chloride electrodes, have a good stability.

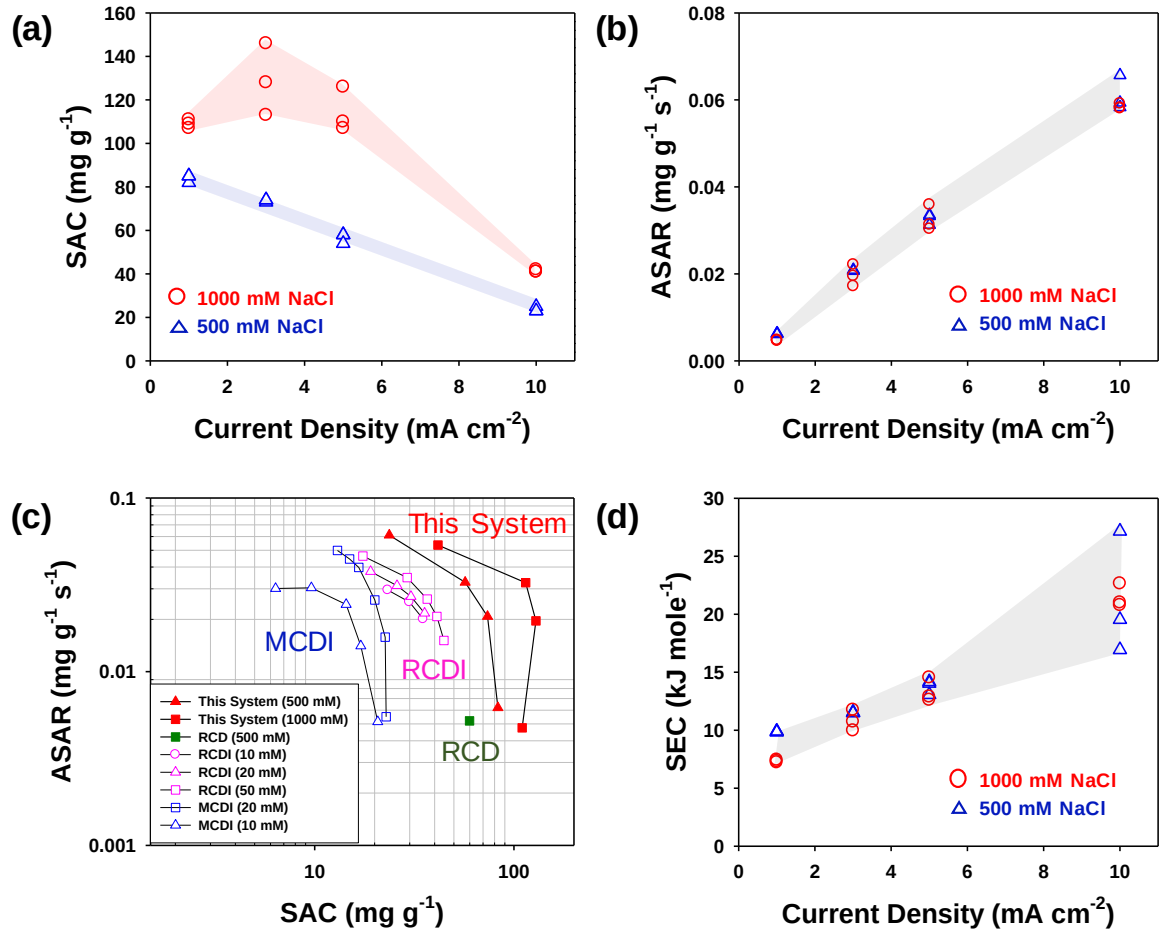

Figure 5. Evaluation of the desalination performance in 500 mM and 1000 mM NaCl solution with different current densities (1.0, 3.0, 5.0, and 10 mA cm^{-2}): (a) salt adsorption capacity (SAC); (b) average salt adsorption rate (ASAR); (c) CDI Ragone plot including various electrochemical desalination system; (d) specific energy consumption (SEC). In (c), MCDI, rocking-chair capacitive deionization (RCDI), and rocking-chair desalination (RCD) data are from ref [27,41,42].

Figure 5 shows the desalination performance of the system with various current densities and different NaCl concentrations examined by providing information on (a) the salt adsorption capacity (SAC), (b) the average salt adsorption rate (ASAR), (c) ASAR plotted versus SAC

which is the “CDI Ragone” plot, and (d) specific energy consumption (SEC). The observed SAC was approx. 85 and 130 mg g^{-1} at 500 and 1000 mM NaCl with current density of 1.0 and 3.0 mA cm^{-2}. These values are much higher than in previous studies with Prussian Blue analogues (approx. 60 mg g^{-1} with 0.5 mA cm^{-2})[27]. The high desalination capacity of the present system results from the inherent high capacity of the silver/silver chloride electrodes and also originates from the design of the cell, which enables desalination during forward current operation, as well as during reverse current operation. However, when the current density was increased, SAC decreased to 30-40 mg g^{-1}. This result is an indication of a limited rate capability in this system, which requires further study to improve ion diffusion or reduce other transport resistances in the system. As shown in **Figure 5a**, the tendency of SAC vs. current density in 1000 mM NaCl is not linear. This result can be explained by the effect of back-diffusion. It is not a negligible effect when the concentration of source water is 1000 mM, and the effect depends on the operation time (**see Figure S5**).

In order to determine the kinetic properties of the system, average salt adsorption rate (ASAR) analysis, which is commonly used in CDI to evaluate the ion removal rate, was conducted. As shown in **Figure 5b**, ASAR progressively increases with current density which shows that it is possible to operate at a high current such as 10 mA cm^{-2}, which is a value that is an order of magnitude higher than previous battery desalination systems which are for instance at 0.5 mA cm^{-2} [20,27,28].

The relationship between the capacity and the rate of desalination is represented by the CDI Ragone plot (**Figure 5c**) [41]. Even though it is difficult to compare with other systems due to differences in salt concentration, our present system exhibits much faster rate and higher capacity than previously reported systems based on MCDI, rocking-chair capacitive deionization (RCDI), and rocking-chair desalination (RCD). For example, our system achieves

a high SAC of around 100 mg g^{-1}, which is a 30% increased value compared to a previous battery desalination study that was conducted at a low ASAR (0.005 mg^{-1} g^{-1} s^{-1}) [27]. In addition, the rate capability of our system was significantly better than in earlier works (we obtain up to 0.05 - 0.06 mg g^{-1} s^{-1}).

To investigate the relationship between current density and specific energy consumption, SEC, our system was run at various current densities in 500 and 1000 mM NaCl solution. As shown in **Figure 5c**, the energy consumption increases as the current density increases. This is because the polarization increases when a higher current flows through a given circuit resistance. In particular, the specific energy consumption in our system was approximately 0.19 Wh L^{-1} (5.3 kJ $mole^{-1}$) at 25% ion removal with 50% water recovery. Even though energy recovery is not possible in our system, see **Figure 5b**, the obtained energy consumption is quite comparable to results reported in other studies [20,27].

Conclusions

In this study, we demonstrate that the high performance of electrochemical water desalination using identical two-phase reaction electrodes (silver and silver-chloride), reducing the cell voltage required for desalination to less than 0.2 V. Even at these low cell voltages, the system achieves a high desalination capacity of approx. 85 mg g^{-1} with 80% of salt removal ratio at 500 mM NaCl solution. Furthermore, the system can operate at a current density (10 mA cm^{-2}) which is an order of magnitude higher than reported for battery desalination systems. We have shown that a high salt adsorption capacity and fast desalination is possible under low voltage operation. With further optimization, we believe that the system proposed in this study can be a feasible desalination technology for treating water of a high salinity.

Acknowledgement

This study was supported by the Basic Science Research Program through the National Research Foundation of Korea (NRF) funded by the Ministry of Education (NRF-2016R1D1A1A02937469), and by the Technology Innovation Program (10082572, Development of Low Energy Desalination Water Treatment Engineering Package System for Industrial Recycle Water Production) funded By the Ministry of Trade, Industry & Energy(MOTIE, Korea)

Reference

[1] S. Porada, R. Zhao, A. van der Wal, V. Presser, P.M. Biesheuvel, Review on the science and technology of water desalination by capacitive deionization, Prog. Mater. Sci. 58 (2013) 1388–1442. doi:10.1016/j.pmatsci.2013.03.005.

[2] M.E. Suss, S. Porada, X. Sun, P.M. Biesheuvel, J. Yoon, V. Presser, Water desalination via capacitive deionization: What is it and what can we expect from it?, Energy Environ. Sci. 8 (2015) 2296–2319. doi:10.1039/c5ee00519a.

[3] C. Tsouris, R. Mayes, J. Kiggans, K. Sharma, S. Yiacoumi, D. Depaoli, S. Dai, Mesoporous carbon for capacitive deionization of saline water, Environ. Sci. Technol. 45 (2011) 10243–10249. doi:10.1021/es201551e.

[4] C. Kim, J. Lee, S. Kim, J. Yoon, TiO2 sol-gel spray method for carbon electrode fabrication to enhance desalination efficiency of capacitive deionization, Desalination. 342 (2014) 70–74. doi:10.1016/j.desal.2013.07.016.

[5] A.C. Arulrajan, D.L. Ramasamy, M. Sillanpää, A. van der Wal, P.M. Biesheuvel, S. Porada, J.E. Dykstra, Exceptional Water Desalination Performance with Anion-Selective Electrodes, Adv. Mater. 31 (2019) 1–5. doi:10.1002/adma.201806937.

[6] C. Kim, J. Lee, P. Srimuk, M. Aslan, V. Presser, Concentration-Gradient Multichannel Flow-Stream Membrane Capacitive Deionization Cell for High Desalination Capacity of Carbon Electrodes, ChemSusChem. 10 (2017) 4914–4920. doi:10.1002/cssc.201700967.

[7] R. Zhao, S. Porada, P.M. Biesheuvel, A. van der Wal, Energy consumption in membrane capacitive deionization for different water recoveries and flow rates, and comparison with reverse osmosis, Desalination. 330 (2013) 35–41. doi:10.1016/j.desal.2013.08.017.

[8] P. Długołecki, A. van der Wal, Energy recovery in membrane capacitive deionization, Environ. Sci. Technol. 47 (2013) 4904–4910. doi:10.1021/es3053202.

[9] M.E. Suss, T.F. Baumann, W.L. Bourcier, C.M. Spadaccini, K.A. Rose, J.G. Santiago, M. Stadermann, Capacitive desalination with flow-through electrodes, Energy Environ. Sci. 5 (2012) 9511–9519. doi:10.1039/c2ee21498a.

[10] S. Porada, L. Borchardt, M. Oschatz, M. Bryjak, J.S. Atchison, K.J. Keesman, S. Kaskel, P.M. Biesheuvel, V. Presser, Direct prediction of the desalination performance of porous carbon electrodes for capacitive deionization, Energy Environ. Sci. 6 (2013) 3700–3712. doi:10.1039/c3ee42209g.

[11] Y.J. Kim, J.H. Choi, Improvement of desalination efficiency in capacitive deionization using a carbon electrode coated with an ion-exchange polymer, Water Res. 44 (2010) 990–996. doi:10.1016/j.watres.2009.10.017.

[12] X. Gao, A. Omosebi, J. Landon, K. Liu, Surface charge enhanced carbon electrodes for stable and efficient capacitive deionization using inverted adsorption-desorption behavior, Energy Environ. Sci. 8 (2015) 897–909. doi:10.1039/c4ee03172e.

[13] C.L. Yeh, H.C. Hsi, K.C. Li, C.H. Hou, Improved performance in capacitive deionization of activated carbon electrodes with a tunable mesopore and micropore ratio, Desalination. 367 (2015) 60–68. doi:10.1016/j.desal.2015.03.035.

[14] S. Il Jeon, H.R. Park, J.G. Yeo, S. Yang, C.H. Cho, M.H. Han, D.K. Kim, Desalination via a new membrane capacitive deionization process utilizing flow-electrodes, Energy Environ. Sci. 6 (2013) 1471–1475. doi:10.1039/c3ee24443a.

[15] J.H. Choi, Determination of the electrode potential causing Faradaic reactions in membrane capacitive deionization, Desalination. 347 (2014) 224–229. doi:10.1016/j.desal.2014.06.004.

[16] T. Kim, J. Yu, C. Kim, J. Yoon, Hydrogen peroxide generation in flow-mode capacitive deionization, J. Electroanal. Chem. 776 (2016) 101–104. doi:10.1016/j.jelechem.2016.07.001.

[17] D. He, C.E. Wong, W. Tang, P. Kovalsky, T. D. Waite, Faradaic Reactions in Water Desalination by Batch-Mode Capacitive Deionization, Environ. Sci. Technol. Lett. 3 (2016) 222–226. doi:10.1021/acs.estlett.6b00124.

[18] B. Shapira, E. Avraham, D. Aurbach, Side Reactions in Capacitive Deionization (CDI) Processes: The Role of Oxygen Reduction, Electrochim. Acta. 220 (2016) 285–295. doi:10.1016/j.electacta.2016.10.127.

[19] J.E. Dykstra, K.J. Keesman, P.M. Biesheuvel, A. van der Wal, Theory of pH changes in water desalination by capacitive deionization, Water Res. 119 (2017) 178–186. doi:10.1016/j.watres.2017.04.039.

[20] M. Pasta, C.D. Wessells, Y. Cui, F. La Mantia, A desalination battery, Nano Lett. 12 (2012) 839–843. doi:10.1021/nl203889e.

[21] H. Yoon, J. Lee, S. Kim, J. Yoon, Review of concepts and applications of electrochemical ion separation (EIONS) process, Sep. Purif. Technol. 215 (2019) 190–207. doi:10.1016/j.seppur.2018.12.071.

[22] J.W. BLAIR, G.W. MURPHY, Electrochemical Demineralization of Water with Porous Electrodes of Large Surface Area, Am. Chem. Soc. 27 (1960) 206–223, doi:10.1021/ba-1960-0027.ch020.

[23] J. Lee, S. Kim, C. Kim, J. Yoon, Hybrid capacitive deionization to enhance the desalination performance of capacitive techniques, Energy Environ. Sci. 7 (2014) 3683–3689. doi:10.1039/c4ee02378a.

[24] S. Kim, J. Lee, C. Kim, J. Yoon, Na2FeP2O7as a Novel Material for Hybrid Capacitive Deionization, Electrochim. Acta. 203 (2016) 265–271. doi:10.1016/j.electacta.2016.04.056.

[25] K.C. Smith, R. Dmello, Na-Ion Desalination (NID) Enabled by Na-Blocking Membranes and Symmetric Na-Intercalation: Porous-Electrode Modeling, J. Electrochem. Soc. 163 (2016) A530–A539. doi:10.1149/2.0761603jes.

[26] S. Porada, A. Shrivastava, P. Bukowska, P.M. Biesheuvel, K.C. Smith, Nickel Hexacyanoferrate Electrodes for Continuous Cation Intercalation Desalination of Brackish Water, Electrochim. Acta. 255 (2017) 369–378. doi:10.1016/j.electacta.2017.09.137.

[27] J. Lee, S. Kim, J. Yoon, Rocking Chair Desalination Battery Based on Prussian Blue Electrodes, ACS Omega. 2 (2017) 1653–1659. doi:10.1021/acsomega.6b00526.

[28] T. Kim, C.A. Gorski, B.E. Logan, Low Energy Desalination Using Battery Electrode Deionization, Environ. Sci. Technol. Lett. 4 (2017) 444–449. doi:10.1021/acs.estlett.7b00392.

[29] J. Ahn, J. Lee, S. Kim, J. Yoon, "An Anion Mediated Rocking-Chair Deionization System" poster presentation at 5th Ertl symposium Nov 23-24, Gwang-ju, Republic of Korea (2018), poster accepted Oct 11 2018.

[30] J. Ahn, J. Lee, S. Kim, J. Lee, J. Yoon, "Rocking-Chair Desalination System Based on Anion Faraday Electrodes" poster presentation at 2019 CDI&E May 20-23, Beijing, China (2019), poster accepted Nov 16 2018.

[31] P. Srimuk, S. Husmann, V. Presser, Low voltage operation of a silver/silver chloride battery with high desalination capacity in seawater, RSC Adv. 9 (2019) 14849–14858. doi:10.1039/c9ra02570g.

[32] E. Bakker, E. Grygolowicz-Pawlak, M. Sohail, B. Neel, R. de Marco, M. Pawlak, A. Shvarev, Coulometric Sodium Chloride Removal System with Nafion Membrane for Seawater Sample Treatment, Anal. Chem. 84 (2012) 6158–6165. doi:10.1021/ac301096r.

[33] M. Fighera, P.D. van der Wal, H. Shea, Microfluidic Platform for Seawater Desalination by Coulometric Removal of Chloride Ions through Printed Ag Electrodes, J. Electrochem. Soc. 164 (2017) H836–H845. doi:10.1149/2.1761712jes.

[34] F. Chen, Y. Huang, L. Guo, M. Ding, H.Y. Yang, A dual-ion electrochemistry deionization system based on AgCl-Na0.44MnO2electrodes, Nanoscale. 9 (2017) 10101–10108. doi:10.1039/c7nr01861d.

[35] P.F. Cai, C.J. Su, W.T. Chang, F.C. Chang, C.Y. Peng, I.W. Sun, Y.L. Wei, C.J. Jou, H.P. Wang, Capacitive deionization of seawater effected by nano Ag and Ag@C on graphene, Mar. Pollut. Bull. 85 (2014) 733–737. doi:10.1016/j.marpolbul.2014.05.020.

[36] L. Wang, S. Lin, Intrinsic tradeoff between kinetic and energetic efficiencies in membrane capacitive deionization, Water Res. 129 (2018) 394–401. doi:10.1016/j.watres.2017.11.027.

[37] A.J. Bard, L.R. Faulkner, Electrochemical Methods: Fundamentals and Applications, Wiley, 2001.

[38] A. van der Ven, M. Wagemaker, Effect of surface energies and nano-particle size distribution on open circuit voltage of Li-electrodes, Electrochem. Commun. 11 (2009) 881–884. doi:10.1016/j.elecom.2009.02.015.

[39] D. Li, H. Zhou, Two-phase transition of Li-intercalation compounds in Li-ion batteries, Mater. Today. 17 (2014) 451–463. doi:10.1016/j.mattod.2014.06.002.

[40] A. van der Ven, J. Bhattacharya, A.A. Belak, Understanding Li diffusion in Li-intercalation compounds, Acc. Chem. Res. 46 (2013) 1216–1225. doi:10.1021/ar200329r.

[41] T. Kim, J. Yoon, CDI ragone plot as a functional tool to evaluate desalination performance in capacitive deionization, RSC Adv. 5 (2015) 1456–1461. doi:10.1039/c4ra11257a.

[42] J. Lee, K. Jo, J. Lee, S.P. Hong, S. Kim, J. Yoon, Rocking-Chair Capacitive Deionization for Continuous Brackish Water Desalination, ACS Sustain. Chem. Eng. (2018) acssuschemeng.8b02123. doi:10.1021/acssuschemeng.8b02123.